Çukurova Üniversitesi
Mühendislik Fakültesi Dergisi
Çukurova University
Journal of the Faculty of Engineering
ISSN: 2757-9255 CİLT/VOLUME: 39 SAYI/ISSUE: 3 EYLÜL/SEPTEMBER 2024

Performance Modeling of the Fenton Process Used as a Single Unit for Treating Raw Textile Effluent

Selman TURKES [1,a], **Hakan GÜNEY** [1,b], **Bülent SARI** [1,c], **Olcayto KESKINKAN** [1,d]

[1]*Cukurova University, Faculty of Engineering, Department of Environmental Engineering, Adana, Türkiye*

[a]***ORCID***: *0000-0001-6420-1002;* [b]***ORCID***: *0009-0003-6991-2569;* [c]***ORCID***: *0000-0002-5171-9491;* [d]***ORCID***: *0000-0001-8995-756X*

Article Info
Received : 10.05.2024
Accepted : 27.09.2024
DOI: 10.21605/cukurovaumfd.1560112

Corresponding Author
Selman TURKES
sidarselman@gmail.com

Keywords
Raw wastewater treatment
Fenton process
ANN
NARX-ANN models
Textile industry

How to cite: *TURKES, S., GÜNEY, H., SARI, B., KESKİNKAN, O., (2024). Performance Modeling of the Fenton Process Used as a Single Unit for Treating Raw Textile Effluent. Cukurova University, Journal of the Faculty of Engineering, 39(3), 679-693.*

ABSTRACT

This study investigates the direct application of the Fenton Oxidation Process (FOP) to untreated textile wastewater, specifically from a woven fabric production facility. Under optimized conditions (pH 3, 0.7 g/L Fe^{+2}, 2 mM H_2O_2), the process achieved significant removal efficiencies: 81% Chemical Oxygen Demand (COD), 80% Suspended Solids (SS), and 93% color removal. Artificial Neural Networks (ANN) and NARX-ANN were utilized in Matlab R2020a to model FOP performance, employing Levenberg-Marquardt (trainlm) and Scaled Conjugate Gradient (trainscg) algorithms. With a 9-20-3 network topology, the ANN model demonstrated superior predictive capability, achieving an R^2 of 0.9843.

Ham Tekstil Atık Sularının Arıtılması İçin Tek Bir Ünite Olarak Kullanılan Fenton Prosesinin Performans Modellemesi

Makale Bilgileri
Geliş : 10.05.2024
Kabul : 27.09.2024
DOI: 10.21605/cukurovaumfd.1560112

Sorumlu Yazar
Selman TURKES
sidarselman@gmail.com

Anahtar Kelimeler
Ham atıksu arıtma
Fenton prosesi
YSA
NARX-YSA modelleri
Tekstil endüstrisi

Atıf şekli: *TURKES, S., GÜNEY, H., SARI, B., KESKİNKAN, O., (2024). Performance Modeling of the Fenton Process Used as a Single Unit for Treating Raw Textile Effluent. Cukurova University, Journal of the Faculty of Engineering, 39(3), 679-693.*

ÖZ

Bu çalışma, Fenton Oksidasyon Prosesinin (FOP) doğrudan arıtılmamış tekstil atık suyuna uygulanmasını, özellikle dokuma kumaş üretim tesisinden gelen atık suyu hedef alarak incelemektedir. Optimize edilmiş koşullar (pH 3, 0.7 g/L Fe^{+2}, 2 mM H_2O_2) altında, proses %81 Kimyasal Oksijen İhtiyacı (KOİ), %80 Askıda Katı Madde (AKM) ve %93 renk giderimi gibi önemli verimlilikler sağlamıştır. FOP performansını modellemek amacıyla Matlab R2020a'da Yapay Sinir Ağları (YSA) ve NARX-YSA modelleri, Levenberg-Marquardt (trainlm) ve Ölçeklenmiş Eşlenik Gradyan (trainscg) algoritmaları kullanılarak oluşturulmuştur. 9-20-3 ağ topolojisine sahip YSA modeli, 0.9843 R^2 değeri ile yüksek bir tahmin yeteneği göstermiştir.

1. INTRODUCTION

Needs for clothing and shelter come right after basic needs such as air, water, and food, which are necessary for the survival of humanity. The increasing demand for textile products for these needs on a global scale has resulted in the textile industry being included in the top five major industrial sectors in the inter-industry classification [1,2]. In addition, as a result of the modeling, it is estimated that the consumption of textile products will increase 3 times worldwide by 2050 [3]. The textile industry, which traditionally consists of stages such as yarn, weaving, spinning, knitting, washing, bleaching, dye-printing, and finishing processes, consumes significant amounts of water and energy According to studies conducted in recent years, stated that over 3 billion tons of [4] wastewater are discharged annually in the textile industry worldwide [5,6]. Textile wastewater is usually processed using procedures such as coagulation, filtration, biological treatment by aerobic means (activated sludge), and adsorption [7,8]. Due to these processes' low efficiency, excessive sludge formation, high initial investment, and operating costs, and an ongoing decline in developed and developing countries' discharge standards (particularly regarding colors), researchers have been working harder over the past 25 years on creating and implementing new and more suitable technology. [9]. One of the areas where these efforts concentrate is Advanced Oxidation Processes (AOP) [10]. (AOPs continue to develop as a highly efficient process, especially for toxic, colored, and biologically treatable wastewater such as textile wastewater. AOPs are efficient, cost-effective, and environmentally friendly treatment processes. It is widely known that AOPs are used in advanced or pretreatment. Researchers and plant operators will be more interested in these procedures when they are used as single-unit systems for wastewater treatment, and this will help to preserve natural water supplies [8,11]. Commonly used AOPs are Fenton, photo-Fenton, ozonation, photocatalysis, radiation, electrochemical oxidation, and sonolysis [12,13]. These procedures are based on the production of hydroxyl radicals (HO•), which have an extremely high 2.80 V oxidation potential. Most organic and pigment compounds can be partially or fully mineralized by radicals [14]. Among these processes, Fenton oxidation stands out with its effectiveness and promising results [14-16]. Henry J. Fenton discovered the Fenton oxidation process (FOP) in 1894. During the 1960s, studies and research on the process were conducted, with a focus on the oxidation of biological pollutants in water, as shown by Equation 1-4 [17-21].

$$Fe^{2+} + H_2O_2 \rightarrow Fe^{3+} + OH^{\cdot} + OH^{-} \quad (1)$$

$$OH^{\cdot} + organics \rightarrow H_2O + inter.products \quad (2)$$

$$OH^{\cdot} + intermediate\ products \rightarrow H_2O + CO_2 \quad (3)$$

$$Fe^{3+} + H_2O_2 \rightarrow Fe^{2+} + HO_2 + H^{+} \quad (4)$$

The FOP begins when divalent iron (Fe^{2+}) in an aqueous solution reacts with hydrogen peroxide (H_2O_2) to form HO• (Reaction 1). Reaction 2 and Reaction 3 produce intermediate products (H_2O and CO_2) and end products (oxidized organic materials in wastewater) respectively, as a result of the generated HO•. A connected reaction cycle is created during oxidation, which further offers Fe^{2+} regeneration, H_2O_2, and Fe^{3+} reactions (Reaction 4). [16,20,22]. When the Fenton process is compared with other AOPs; It has many advantages such as being simple to apply, not requiring special ambient conditions, high speed and amount of HO• formation, high oxidation capacity, relatively low cost, the wide area of use and being environmentally friendly [16,21]. In addition, the ferrous sewage that develops in the final phase is the main drawback of the FOP. Separation and disposal of this sludge cause additional costs [23]. In addition, dissolved Fe^{2+} remaining in treated water can cause problems during water reuse, especially in the textile industry, and may require additional treatment processes [24].

Numerous factors including pH, H_2O_2, and Fe^{2+} dose, interaction and reacting period, the flow rate, reactor quantity, temperature outside, and effluent quality all affect how well FOP performs when used in the advanced treatment of textile wastewater. The complexity of the reactor's response phases and a wide range of factors make it difficult to estimate efficiency and optimize the FOP using conventional approaches, wasting time and raising the cost of process design and scaling [25-28]. To make the design and operation of the FOP highly effective, applicable, current, and future-oriented, as well as more economical, optimization and modeling studies are becoming increasingly important [27,29]. The environmental engineering discipline has extensively studied and applied modeling techniques in water and wastewater treatment operations. Adaptive Neural Fuzzy Control System (ANFIS), the Surface Responsive Method (RSM), the method of Multiple Linear Regression (MLR), and Artificial Neural Networks (ANN), among

others, are the most often used [8]. ANN is one of the most significant models used nowadays, particularly in the scientific and engineering domains, to establish the connection among operating factors influencing numerous procedures and equipment outputs [25,26,28,30]. Based on the organic neuron system, artificial neural networks (ANN) are statistical methods of modeling that aim to provide novel information using brain-specific skills [28,29,31]. In terms of generating algorithms for existing information not requiring over previous layout and modification [8], simplification of modeling, calculation, as well as predicting [25], illuminating the relationships between factors and the outcomes [26], adaptability, forecasting efficiency, and user-friendliness, this approach is thought to be a promising tool [29]. One of the time-series studies is the Nonlinear External Input Autoregressive Artificial Neural Networks (NARX-ANN) model, in addition to the ANN approach. One form of dynamic filter is the time series evaluation, which uses past data to forecast future data. Numerous systems, including heat exchangers, wastewater treatment, manufacturing equipment, processes related to chemicals, automation, and aviation mechanisms, are subject to evaluation, modeling, tracking, and operation using this software [32,33].

The FOP is typically used for enhanced or prior treatment, in which case the treatment plants will produce both chemical and biological sludge. Only chemical sludge will occur when the FOP is utilized for only one process for treatment in basic textile waste stream treatment; overall, sludge formation will likely be lower than with combination treatment alternatives. The experimental results regarding the FOP process's ability to remove COD, SS, and color in unprocessed wastewater from textiles are provided in this study. FOP has simple and fast reactions, low cost and environmental friendliness. In addition, models that can predict the performance of processes have been developed and compared by artificial intelligence models (ANN and NARX-ANN), which are one of the areas of focus in studies on AOPs in recent years. Seldom is a study conducted in the literature that treats raw wastewater from textile manufacturing using the FOP as only one component and compares the process's performance to that of ANN and, in particular, NARX-ANN models. The study's findings provide crucial information for the global treatment of textile wastewater in the interest of sustainable development. As a result, investigators and managers in treatment facilities may be interested in this research.

2. MATERIALS AND METHODS

2.1. Raw Textile Effluent

Table 1 lists the general features of the unprocessed wastewater from textile industries and the statistical assessment of each sample utilized in the FOP. A local textile plant that was established in Adana, Turkey, and produced woven fabrics provided the untreated textile effluent used in the study.

Table 1. Heterogeneous pollutant features and statistical analysis of untreated water used for fabric waste in the FOP

	pH	COD	SS	Color	Temp	EC
Sample number	**20**	**20**	**20**	**20**	**20**	**20**
Mean	9.80	1341.15	100.05	1395.00	45.00	1463.00
Median	9.80	1341.50	99.50	1396.00	45.00	1464.50
Mode	**9.80**	**1341.00**	**97.00[a]**	**1396.00**	**45.00[a]**	**1462.00[a]**
Std. dev.	0.12140	10.09051	5.65197	6.00877	2.02614	12.66574
Variance	0.015	101.818	31.945	36.105	4.105	160.421
Minimum	9.50	1315.00	89.00	1382.00	41.00	1437.00
Maximum	10.00	1357.00	117.00	1408.00	48.00	1492.00
Sum	196.00	26823.00	2001.00	27900.00	900.00	29260.00

[a] There are several modes. The value that is the smallest is displayed.

2.2. Analytical Method

The MERCK brand of analytical purity chemicals is utilized in the experimental investigation, H_2O_2 as oxidant and $FeSO_4.7H_2O$ as a catalyst in the FOP process; NaOH and H_2SO_4 for pH adjustments; For COD analysis, $K_2Cr_2O_7$, $(NH_4)_2Fe(SO_4)_2.6H_2O$, 1.10-Phenontrolline monohydrate, $HgSO_4$ and Ag_2SO_4 were used. Fast mixing, slow mixing and settling were carried out in the Jar-Test device (MTOPS SF4). pH measurements were made with

OHAUS, WTW conductivity meter was utilized to determine electrical conductivity (EC), DS/890 colorimeter was used with color measurements, HACH LANGE DR 6000 was applied in COD

measurements, and Whatman GF/C was employed as SS measurements. All analyses were conducted using techniques based on Standard Procedures [34]; three repetitions of the analyses were carried out, and the arithmetic mean of the data was used. The methods applied were COD (5220 C), AKM (2540 D), Color (2120 C), pH (4500-H+ B), Temperature (2550 B), and Electrical Conductivity EI (2510 B).

2.3. FOP Experiments

Under laboratory circumstances, FOP experimental studies were conducted in a jar testing setup depicted in Fig. 1. To prevent light from affecting the experimental setup, it was housed in a cardboard box that was covered in aluminum foil. Five minutes of fast mixing (250 rpm), sixty minutes of slow mixing (50 rpm), and sixty minutes of settling times were used in studies filling bottles containing 700 mL of untreated fabric waste with a volume of 1000 mL. pH was adjusted at intervals of 2.0–7.5; Fe^{2+} was added at 0.15–1.05 g/L; and H_2O_2 was added at 1–12 mM. To start oxidation, the catalyst (Fe^{2+}) and oxidant (H_2O_2) were added to the beaker quickly. 1N H_2SO_4 and NaOH solutions were then used to correct the ambient pH. After the oxidation step, the pH was raised to 8.5 to guarantee sufficient slow stirring & flocculation itself were carried out, and precipitation was used to finish the FOP process.

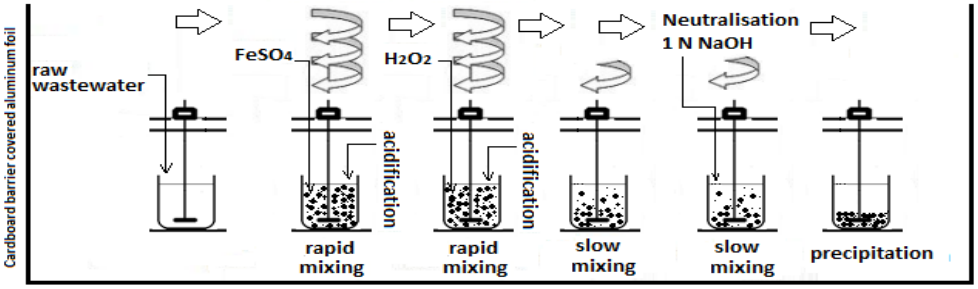

Figure 1. Schematic of the FOP experimental steps

Following the precipitation process, samples were taken from the beaker's top phase, and each assessment group was carried out on three separate occasions with COD, SS, and color analyses performed. The entire procedure was conducted at 25±2 ºC ambient temperature and pressure in the air.

2.4. Methods for ANN and NARX-ANN

Table 2 displays the model technique scheme used in this investigation.

Figures 2 and 3 illustrate the architecture of the ANN and NARX-ANN, respectively, showcasing the interplay between input and output layers. Following the outlined methodology, the FOP inputs for both models encompass pH, Fe^{2+} concentration (g/L), H_2O_2 dosage (mM), treatment duration (min), temperature (°C), fast and slow mixing rates (rev/min), sample volume (mL), and electrical conductivity (EC) measured in µS/cm. Meanwhile, the outputs comprise COD, AKM, and Color parameters. In the models, tested with neuron counts ranging from 2 to 20 in increments of 2, a total of 396 (9x44) inputs and 132 (3x44) output datasets were incorporated for ANN and NARX-ANN, respectively. These datasets were divided into three categories: training (70%), validation (15%), and testing (15%).

Table 2. The framework of the FOP model technique

Unprocessed Waste from Fabrics		
COD, SS, and Color in the Fenton Method		
Model	**ANN**	**NARX-ANN**
Directives	nntool	nnstart-ntstoll
Category of network	Feedforward backprop	Feedback Loop
Algorithm for training	Trainlm, Trainscg	Trainlm, Trainscg
Adaptive learning process	LEARNGDM	LEARNGDM
Network attribute	%70 Training, %15Validation, %15 Test	%70 Training, %15Validation, %15 Test
Performance function	MSE	MSE
Regression	R	R
The number of layers	2	2
Quantity of neurons	2-20 (2 each)	2-20 (2 each)
Transfer function	TANSIG, LOGSIG	TANSIG

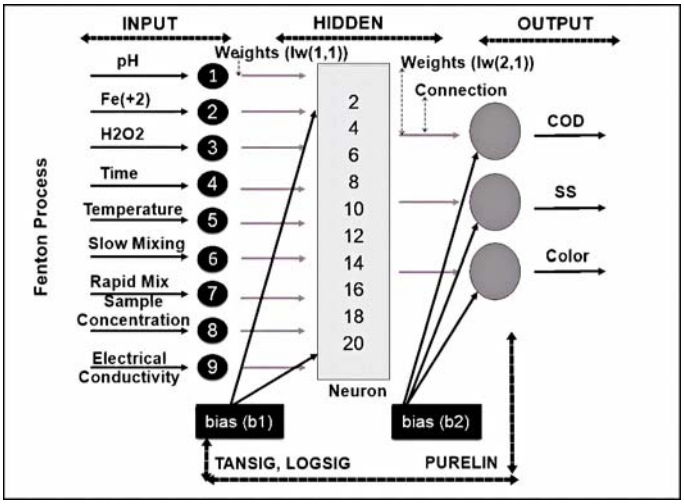

Figure 2. Illustrates the architecture of the constructed ANN model

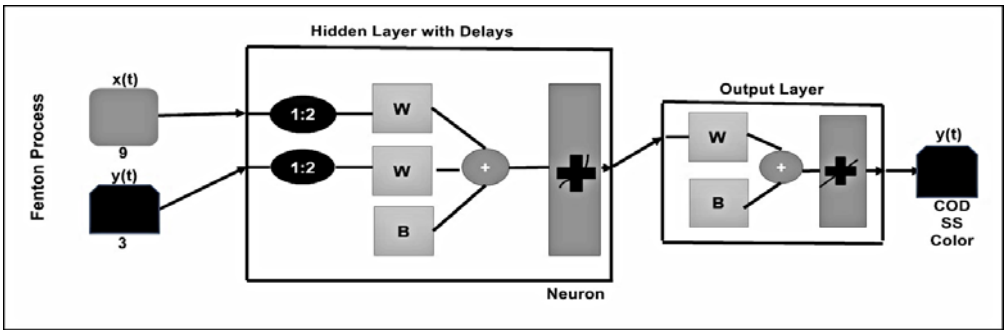

Figure 3. Illustrates how the resulting NARX-ANN algorithm was designed

Several activation functions were used in the study at various neural network levels. In particular, the Purelin function was used in the output layer of the ANN, and ın the unseen layer, Tansig as well as Logsig algorithms were employed. In the same way, Purelin functions were employed in the output layer and Tansig functions in the hidden layer of the NARX-ANN model. In the training phase, 1000

epochs of weight and trend adjustments were performed by comparing two different algorithms, "trainlm" and "trainscg." To enhance convergence and manage nonlinearities, momentum-weighted descent of gradients and a biased learning function (LEARNGDM) were added to the ANN and NARX-ANN training processes.
Notably, "trainlm," renowned for its rapid and stable convergence [35-38], is adept at solving nonlinear challenges based on the Hessian Matrix (equation 5) [33,39,40].

$$\Delta w = [J^T(w)\, J(w) + \lambda I]^{-1}\, J^T(w)\, e(w) \tag{5}$$

In Equation 1, The mass of the vector is represented by *w.*; *J*, Jacobian matrix; J^T, overturned; *Iw*, identity matrix; λ is the value of the learning stable, while with represents an error vector, Equation 1 is adjusted iteratively to find the minimum error. As discovered by Møller [41], the Scaled Conjugate Gradient (trainscg) weight can train any network as long as its net input and transfer functions have derivative functions [41-43]. According to the equation adapted by Du and Stephanus [40,44];

$$\Delta w = w_k - w_{k-1} = \alpha_k d_{k-1} \tag{6}$$

In Equation 6, the number that represents the number of iterations is k.; α_k is defined as the stride length in the k iteration and d_{k-1} is the search direction.

Equation 7 in the range of “mapminmax” (-1,1) was used in the scaling optimization of the inputs and outputs in the models [45]:

$$y = \frac{(y_{max}-y_{min})(x-x_{min})}{(x_{max}-x_{min})} + y_{min} \quad (7)$$

In Equation 7, x_{max} and x_{min} reflect the data's highest and lowest values, while y_{max} and y_{min} take the values 1 and -1, respectively. y is the normalization of x. The problem definition of the NARX-ANN model is expressed by Equation 8 [40,46].

$$y(t) = f\big(x(t-1), x(t-d), y(t-1)y(t-d)\big) \quad (8)$$

In the equation, x(t-d) represents the input, y(t-d) represents the network outputs; d indicates the value of the past inputs and outputs to be used in the feedback. R^2 the MSE were considered in order to assess how well the projected values in each model performed [47,48].

$$R^2 = 1 - \frac{\sum_{i=1}^{N}(y_{thm,i} - y_{dny,i})^2}{\sum_{i=1}^{N}(y_{thm,i} - y_{ort})^2} \quad (9)$$

$$MSE = \frac{1}{N}\sum_{i=1}^{N}(|y_{thm,i} - y_{dny,i}|)^2 \quad (10)$$

In Equations 9 and 10, N is the number of data; $y_{thm,i}$ is the expected predictive value; $y_{dny,i}$ represents the true value, the mean value of the true samples.

3. RESULTS AND DISCUSSION

3.1. Results of FOP Experiments

3.1.1. Effect of pH

Figure 4 shows how different pH values affect the Fenton oxidization procedure and how COD, SS, and color parameters change as the outcome. The study investigated pH values that extend from 2.0 to 7.5 while keeping constant Fe^{2+} and H_2O_2 dosages of 0.15 g/L and 1 mM, respectively. The most significant removal rates were achieved at pH 3, resulting in 72% COD reduction, 76% SS removal, and 90% color elimination. Previous research on FOP has consistently emphasized the pivotal role of pH in influencing the process dynamics. The acidic conditions fundamental to FOP are instrumental in regulating HO• formation, oxidation rates, and the simultaneous control of Fe^{2+} and H_2O_2 doses.

According to Figure 4, there is a decrease in the values of the parameters measured in the wastewater as the pH 3 value goes to the left and right.

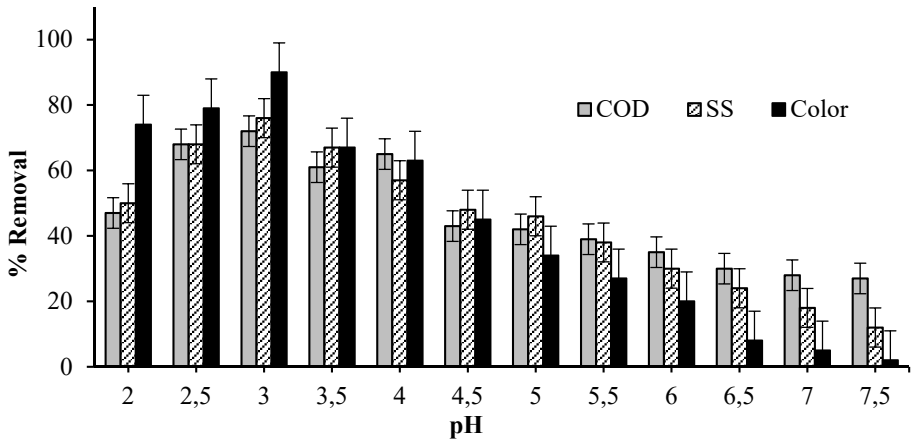

Figure 4. Graph for showing the effect of pH on FOP performance

At pH levels below 3, characterized by elevated H^+ ion concentrations, there's an increased tendency for H_2O_2 to convert into the oxonium ion ($H_3O_2^+$). This conversion enhances the stability of H_2O_2, thereby slowing its reaction with Fe^{2+} ions. Consequently, the formation of complex iron compounds occurs instead of Fe^{3+}, disrupting the $[Fe(H_2O)_6^{2+}]$-FOP cycle. Moreover, according to Pliego et al. [57], heightened H^+ ion concentrations hinder HO• radical formation due to their scavenging effect. Conversely, at pH levels above 3, the reaction rate between Fe^{2+} and H_2O_2 diminishes, resulting in the formation of $Fe(OH)_3$. This formation impedes Fe^{2+} regeneration and diminishes the catalyst's presence in the environment, consequently reducing treatment efficiency. Furthermore, Roudi et al. [50] pointed

out that H_2O_2 becomes more unstable in alkaline solutions, which could cause it to break down into molecules of water and oxygen and impair the FOP's ability to oxidize. In light of this information, the study's findings align meaningfully with existing literature, providing valuable insights into the process.

3.1.2. Impact of Fe^{2+} Content

The measurements of COD, SS, and Color detected in the effluent were utilized to assess the impact of Fe^{2+} material on FOP performance. This was accomplished by studying several Fe^{2+} concentration ranges (0.15-1.05 g/L) at constant pH and H_2O_2 concentrations (pH 3 and 1 mM H_2O_2) (Figure 5).

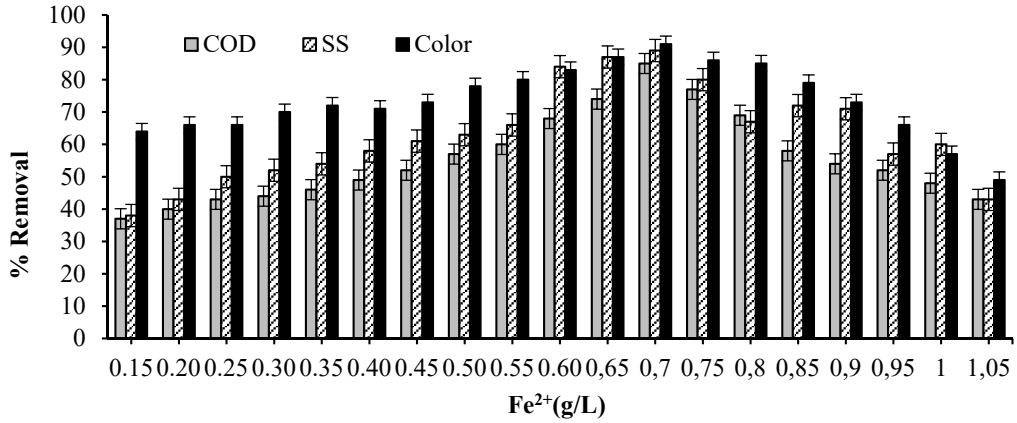

Figure 5. Fe^{2+} concentrations' impact on textile wastewater's ability to remove color, SS, and COD

Fenton-like Oxidation Process (FOP) treatment of untreated textile effluent at 0.7 g Fe^{2+}/L was shown to be the ideal concentration based on research findings. At this concentration, notable clearance

rates of 80% for COD, 79% for SS, and 91% for color were attained. Figure 5 illustrates how increasing the Fe^{2+} dosage from 0.15 g/L to 0.7 g/L resulted in enhanced removal rates for COD, AKM, and color, elevating them from 40-60% to 80-90%. This trend underscores the heightened generation of HO radicals with increased Fe^{2+} dosage, consistent with findings by Abedinzadeh et al. [59] and Roudi et al. [50]. Conversely, a decline in removal rates to 50-60% was observed at Fe^{2+} doses between 0.7-1.05 g/L. This decrease is attributed to the inhibition of HO radicals by excess Fe^{2+} concentrations exceeding 0.7 g/L, in line with studies by [32,49,50]. Furthermore, as noted by Sevimli et al. [60], the formation of Fe^{3+} (Equation 1) in the Fenton process can react with H_2O_2 to generate Fe^{2+} and hydroperoxyl radicals (HO_2•) (Equation 4), thereby depleting H_2O_2 concentration and impeding HO• formation and efficacy. Hence, excessive Fe^{2+} utilization leads to unnecessary chemical consumption, excessive sludge formation, and compromised process efficiency.

3.1.3. Effect of H_2O_2 Concentration

When Fe^{2+} is catalyzed and the environment is acidic, H_2O_2 in the FOP forms a greater HO• radical than it does. That being said, one of the key factors influencing the effectiveness of the procedure is the concentration of H_2O_2. The effective concentration was ascertained in this work by testing a range of H_2O_2 values, from 1 to 12 mM, at a fixed pH and Fe^{2+} concentration (pH 3 and 0.7 g/L) (Fig. 6). For COD, SS, and color at 2 mM H2O2 concentration, the greatest efficiency of removal was 81%, 80%, and 93%. There

was a double rise in the concentration that was effective at the start (from 1 mM to 2 mM), which led to increases in COD removal of 12%, SS reduction of 73%, and color elimination of 20%.

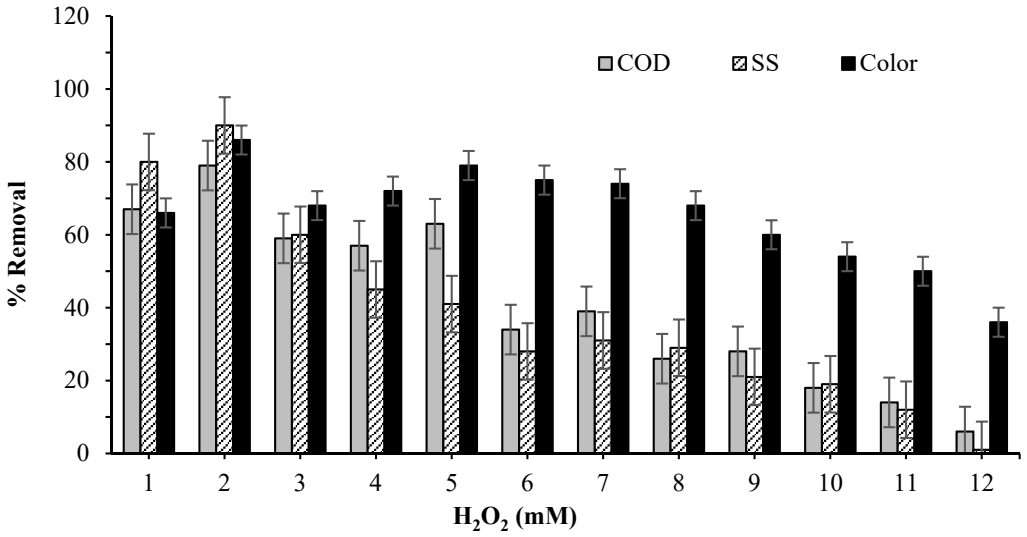

Figure 6. FOP performance: effect of H_2O_2 concentrations

The color parameter of the untreated water employed in this study, which had an average original color concentration of 1395 Pt-Co, drops to about 98 Pt-Co as a result of the 93% color removal. It follows that nearly all of the discharge requirements listed in Table 3 can be satisfied with FOP.

Table 3. Guidelines related to a particular brand and minimum color levels for discharge waters regulated by different nations [61]

Countries and companies	Regulation limits
Turkey (fabric),	280 Pt-Counits
Taiwan (fabric),	550 Pt-Counits
India (dye and dye business),	400 Pt-Counits
Malaysia (industrial, used for drinking water),	100 Pt-Counits
Vietnam (textile, used for drinking water),	50 Pt-Counits
Vietnam (industrial, used for domestic water),	20 Pt-Counits
China (textile, direct discharge),	Follows a dilution method not Pt-Counits
Italy (industrial)	Follows a dilution-method not Pt-Counits
India (industrial, surface waters),	Absent of color
Thailand (textile),	Not objectionable
South Korea (industrial, type I area),	200 chromaticitydegree
Nike,	150 Pt-Counits
C&A (follows BSR),	150 Pt-Counits
H&M (follows BSR),	150 Pt-Counits
New Balance (follows BSR),	150 Pt-Counits
Levi Strauss &Co.,	Not offensive

The elimination effectiveness increases in tandem with the initial H_2O_2 concentration. This suggests that a large and swift production of the HO_2• radical is needed for the oxidative degradation of contaminants in raw textile effluent [32,49]. Nevertheless, as Fig. 6 illustrates, there was no evidence of a fully linear correlation between this rise and the effectiveness of removal. In a range of 2–12 mM, a non-uniform declining trend in removal rates was noted at H_2O_2 concentrations. Addressing the topic, Abedinzadeh et al., [59] claimed there was a decline, while Mousavi et al., [49] claimed that raising the H_2O_2 concentration. did not significantly alter the removal rates. The explanation for this decrease is that using more H_2O_2 than necessary leads to generating hydroperoxyl radical (OOH•), which has a lesser oxidation capacity. As a result, the rate of HO• radical formation declines [55,59,62,63].

The greatest efficiency of the process in this investigation was achieved at pH 3, 0.7 Fe^{2+} g/L, and 2 mM H_2O_2 concentrations, with 81% COD, 80% SS, and 93% color removal. Examining the research on FOP, it becomes clear that SS is not the main focus—rather, organic matter (as COD) and dyestuff (Color) oxidation dominate. The primary cause of this is that, rather than using actual textile effluent, the research reported in the literature was conducted using synthetic wastewater or water dye solutions. FOP is a three-step process that involves the flocculation and precipitation phases. It is based on the oxidation process. An important factor to consider while evaluating is the efficacy of the flocculation and subsequent settling processes, particularly the quantity of suspended solids (SS). This work closes some of the existing information gaps in the sector by using untreated textile wastewater alongside SS for wastewater monitoring. It will make it possible to use the collected data more suitably and helpfully.

3.3. Building a Model and Accurate Predictions

The following tables provide comparative statistical parameters of the ANN and NARX ANN models that were created utilizing the Fenton process variables: Tables 4, 5, and 6. To determine the ideal number of neurons, a range of 2 to 20 was added to the models, as there is no set network architecture or neuron count. Traditional training algorithms used in ANN and NARX-ANN; Scaled Conjugate Gradient (SCG), Bayesian Regularization (BR), Broyden-Fletcher Goldfarb-Shanno (BFGS) and Levenberg-Marquardt (LM). For the most part, studies have chosen to use logistic regression (LM), one of the most used classical training techniques that uses quadratic derivatives [30,64,65]. The LM and SCG algorithms were applied and contrasted in this work. A 70% training, 15% validation, and 15% test set of data were employed for the LM and SCG algorithms. This study compared ANN and NARX-ANN using MSE and R^2 values. When R^2 is assessed between 0 and 1, it indicates, in percentage terms, how well the values of the variables identified or targeted at each stage of the model were estimated. The model is more efficient when the value is near 1. The prediction efficiency increases with the MSE's proximity to zero, so it's usually positive [31,45,66,67].

Table 4. Results of ANN model LM learning algorithm

Using the fenton ANN-nntool-levenberg marquardt algorithm (trainlm), COD-SS-Color, and MSE-R											
		TANSIG function					LOGSIG function				
			Regression (R)					Regression (R)			
ANN structure	Epoch	MSE	Training	Validation	Test	All	MSE	Training	Validation	Test	All
9-2-3	1000	68.9	0.9233	0.94716	0.88982	0.92261	43.5	0.92757	0.84043	0.87202	0.89855
9-4-3	1000	18.0	0.91235	0.85262	0.89784	0.88768	32.8	0.93799	0.24007	0.93373	0.88649
9-6-3	1000	2.98	0.98184	0.72014	0.97021	0.94832	8.29	0.76041	0.98667	0.9409	0.82135
9-8-3	1000	60.2	0.94065	0.80909	0.67778	0.90468	3.65	0.98135	0.97238	0.94669	0.97814
9-10-3	1000	0.432	0.99224	0.94334	0.934	0.97889	754	0.56349	0.68857	0.69365	0.59943
9-12-3	1000	0.0642	0.99689	0.93356	0.9243	0.98247	0.0379	0.99148	0.99304	0.95511	0.98836
9-14-3	1000	666	0.60259	0.70777	0.16507	0.57516	650	0.56708	0.38652	-0.22918	0.47728
9-16-3	1000	0.0998	0.96974	0.9816	0.99863	0.97725	0.143	0.90397	0.98503	0.83596	0.91054
9-18-3	1000	72.1	0.81896	0.8486	0.90431	0.83191	0.108	0.92509	0.9826	0.93881	0.93184
9-20-3	1000	1.08e+03	0.5138	0.53508	0.34276	0.45442	8.84e-09	0.99709	0.96609	0.98737	0.99212

Table 5. ANN model SCG learning algorithm results

COD-SS-Color and MSE-R using fenton ANN-nntool-scaled conjugate gradient algorithm (trainscg)											
		TANSIG function					LOGSIG function				
			Regression (R)					Regression (R)			
ANN structure	Epoch	MSE	Training	Validation	Test	All	MSE	Training	Validation	Test	All
9-2-3	1000	61.7	0.8921	0.85079	0.63952	0.86375	49.4	0.92873	0.92432	0.82046	0.91973
9-4-3	1000	17.4	0.97109	0.94654	0.59935	0.91747	50.5	0.83116	0.97472	0.96669	0.86839
9-6-3	1000	11.2	0.90876	0.95556	0.96914	0.9267	9.63	0.94734	0.92528	0.78838	0.92888
9-8-3	1000	10.1	0.96419	0.98484	0.79142	0.92116	6.55	0.97421	0.98278	0.73807	0.95169
9-10-3	1000	6.8	0.9582	0.56225	0.87667	0.90487	4.96	0.96365	0.93871	0.99427	0.96753
9-12-3	1000	4.29	0.94725	0.97105	0.99097	0.9585	6.79	0.9608	0.86381	0.96715	0.94128
9-14-3	1000	3.41	0.99138	0.99393	0.99624	0.99272	3.12	0.95884	0.97424	0.88232	0.9489
9-16-3	1000	3.39	0.97723	0.98715	0.94778	0.9734	3.88	0.97372	0.99593	0.94391	0.97675
9-18-3	1000	833	0.62612	-0.29346	0.40781	0.53607	3.81	0.96981	0.99603	0.87859	0.96686
9-20-3	1000	3.91	0.97401	0.98419	0.9864	0.97774	2.19	0.97204	0.93112	0.99214	0.97336

Table 6. NARX-ANN model LM and SCG learning algorithm results

MSE-R and fenton NARX-ANN-nnstart-COD-SS-Color												
	Levenberg marquardt algorithm (trainlm)						Scaled conjugate gradient algorithm (trainscg)					
	TANSIG-purelin function											
NARX-ANN structure	Epoch	MSE	Regression (R)				Epoch	MSE	Regression (R)			
			Training	Validation	Test	All			Training	Validation	Test	All
9-3-2-3	9	62	0.78246	0.81323	0.83693	0.79986	46	106	0.87087	0.90221	0.65224	0.82195
9-3-4-3	20	8.08	0.99044	0.93793	0.58931	0.92036	22	74.2	0.90912	0.77757	0.74079	0.8729
9-3-6-3	18	1.81	0.99467	0.93253	0.78738	0.94379	15	70.9	0.90137	0.90617	0.64499	0.85801
9-3-8-3	12	0.737	0.98136	0.90008	0.79946	0.94637	22	57.2	0.92437	0.89967	0.68175	0.89028
9-3-10-3	9	17.1	0.92927	0.62293	0.79562	0.88813	18	75.8	0.89808	0.6937	0.84686	0.86214
9-3-12-3	10	1.62	0.96286	0.87354	0.83727	0.92575	22	55.1	0.92983	0.96254	0.68709	0.87708
9-3-14-3	10	6.46	0.51673	0.54831	0.39359	0.51071	84	4.46	0.99298	0.94068	0.79606	0.93628
9-3-16-3	9	0.613	0.9702	0.8487	0.97289	0.96314	41	29.3	0.95914	0.97759	0.22099	0.87169
9-3-18-3	10	1.09	0.95511	0.42037	0.89501	0.83782	18	39.9	0.93737	0.46815	0.78382	0.86966
9-3-20-3	12	10.1	0.96922	0.63541	0.64176	0.82724	21	35.7	0.93631	0.79207	0.78648	0.89421

When the developed ANN (Table 4-5) model is compared considering the MSE and R^2 results. in the Logsig transfer function of the Levenberg-Marquardt learning algorithm in the 9-20-3 network topology; R^2 values for MSE $8.84e^{-9}$. Training, Validation, Test and All were calculated as 0.9942, 0.9333, 0.9748, 0.9843, respectively. For the NARX-ANN model (Table 6). MSE 0.613 in 9-3-16-3 network topology. and R^2 values are calculated as 0.9412, 0.7202, 0.9465 and 0.9276 for the same algorithm respectively. Figures 7 and 8. respectively. display the regression (R) graphs created for the developed models. The graphs have estimated values on the Y-axis and experimental data on the X-axis. The fit line illustrates the correlation between the estimated value and the input data. The goal line or Y=T line is reached when the estimated and actual values are equal. The COD, color, and SS parameter values that were acquired from the experimental FOP are represented numerically as the "Data" indicator [68]. Considering Figure 7-8. the experimental performance of the Fenton process in raw textile wastewater and the performance estimation made using the created models are summarized in Table 7 for the COD, SS, and Color parameters.

As can be seen in Table 7 the experimental, and estimated removal results in the developed ANN model are more compatible than NARX-ANN. It is also seen that H_2O_2 is more effective in Fenton process performance than pH and Fe^{+2}. Similarly, Huo et al. [69], stated that the effective removal in the Fenton process would be very poor without the addition of H_2O_2. Because H_2O_2 ion provides HO radical formation. which is the main element of the Fenton oxidation process under Fe^{+2} catalysis and acidic conditions [16,50,63]. Yu et al. [70], obtained an estimation ranging from 0.91-0.99 R^2 with the ANN model they developed in 5-4-1 net structure for the estimation of COD and Color removal from synthetic textile wastewater with FOP. Accordingly, it is possible to say that the ANN model with 0.9843 R^2 and 8.84e-9 MSE obtained in this study in the 9-20-3 net topology for the performance estimation of FOP for raw textile wastewater treatment is successful.

The NARX-ANN model developed in the 9-3-16-3 network topology in the study has 0.9276 R^2 and 0.613 MSE. The difference between the experimental and estimation results is higher for pH. Fe^{+2} and H_2O_2 than for the ANN. According to the direction of information flow and processing. ANNs are organized in layers with a one-way information flow in feedforward neural networks (FNN). while in networks with repetitive features such as NARX-ANN. information can be directed both forward and backward. allowing connections between neurons in the same or previous layers flows [32,40,71,72]. Therefore, the NARX-ANN estimation performance is considered to be weaker due to the high number of input/output parameters, the reuse of the output data together with the input data, the repetitive neuron networks in the training of the model, and the low number of epochs.

Although there are no ANN and NARX-ANN modelling studies in the treatment of raw textile wastewater with the FOP in the literature. studies have been found for estimating the thermal damping effect in underground vertical shafts [73], and estimating the groundwater level [40]. In both studies, it was reported that MSE values close to zero and R^2 values above 0.9 were obtained. The prediction performances obtained as a result of the application of the NARX-ANN model in different areas show that the model is within acceptable limits.

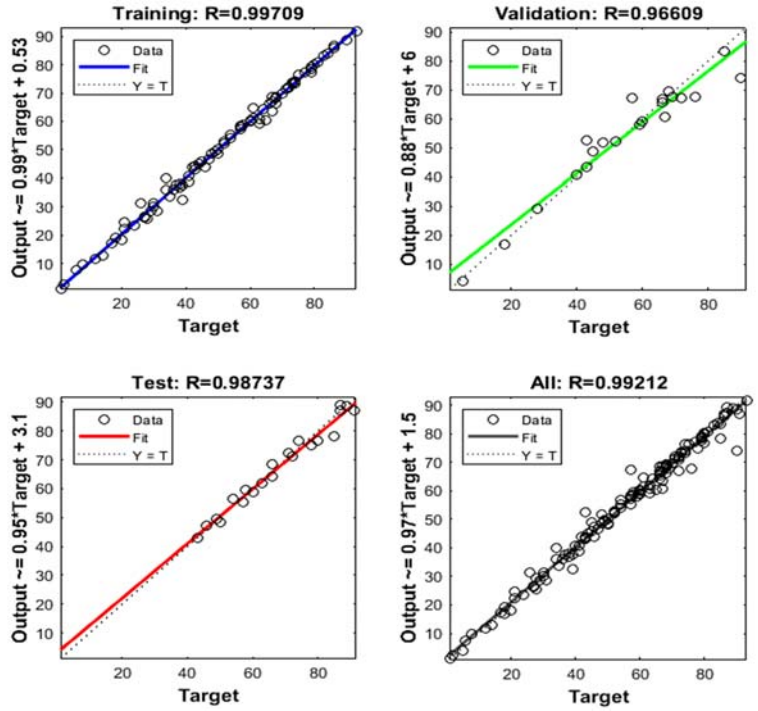

Figure 7. LM algorithm regression results of ANN

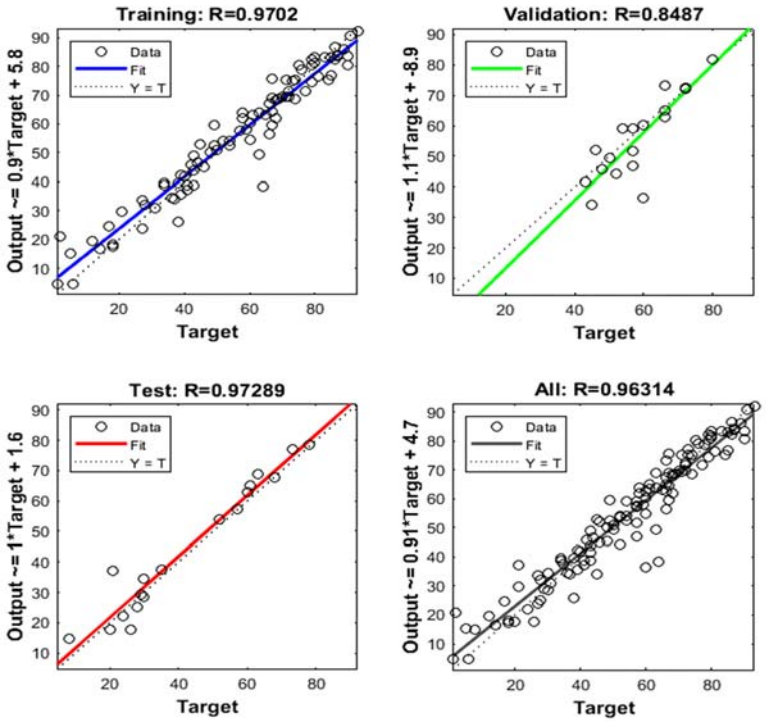

Figure 8. LM algorithm regression results of NARX-ANN

Table 7. Fenton process performance and estimation in unprocessed textiles waste

pH	Fe^{+2} (g/L)	H_2O_2 (mM)	Actual removal (%)			Predict removal (ANN) (%)			Predict removal (NARX-ANN) (%)		
			COD	SS	Color	COD	SS	Color	COD	SS	Color
3	0.15	1	72	76	90	67.14	67.79	74.12	80.26	80.57	86.59
3	0.7	1	80	79	91	78.22	88.75	87.04	76.44	83.30	92.04
3	0.7	2	81	80	93	80.80	79.98	91.72	63.20	57.63	63.77

4. CONCLUSION

To ascertain the effective removal effectiveness of FOP applied to raw textile wastewater and to forecast the performance efficiency, the following study constructed and compared the ANN and NARX-ANN models. The FOP operated at its peak efficiency at pH 3, 0.7 Fe^{2+} g/L and a 2 mM H_2O_2 concentration. Under these circumstances, 81%, 80%, and 93% of the COD, SS, and color were removed, respectively. COD, SS, and color removal increased from 40–60% to 80–90% with the increase in Fe^{2+} dose from 0.15 g/L to 0.7 g/L. However, at dosages between 0.7 and 1.05 g/L, the removal rates decreased from 80–90% to 50–60%. Excessive sludge development and needless chemical usage are the results of using too much Fe^{2+}. It has been established that the application of FOP as a single unit can satisfy the receiving environment discharge standards specified for wastewater from the textile sector. taking into account the properties and treatment efficiencies of basic textile wastewater. Furthermore. it was found that the Artificial Neural Network model performed better and with greater

reliability when the MSE and R^2 values of the ANN and NARX-ANN models created for FOP were compared. For ANN. the R is 0.9843 and the MSE is 8.84e-9. The experimentally observed removal rates show a good agreement with the model estimations. Further research can be conducted to compare the prediction performances of regression models with ANN models by analyzing the data and models.

5. ACKNOWLEDGEMENT

This study was supported by the Çukurova University Scientific Research Projects Unit with the project number FYL-2018-9993.

6. REFERENCES

1. ABIT, 2018. Brazilian textile and apparel industry association. Brazilian Textile and Apparel Industry. Brasília, 44.
2. Sher, F., Hanif, K., Iqbal, S.Z., Imran, M., 2020. Implications of advanced wastewater treatment: electrocoagulation and electroflocculation of effluent discharged from a wastewater treatment plant. Journal of Water Process Engineering, 33, 101101.
3. Alkhagen, M., Samuelsson, Å., Aldaeus, F., Gimåker, M., Östmark, E., Swerin, A., 2015. Roadmap 2015 to 2025. Textile Materials from Cellulose. RISE–Research Institutes of Sweden.
4. He, X., Qi, Z., Gao, J., Huang, K., Li, M., Springael, D., Zhang, X.X., 2020. Nonylphenol ethoxylates biodegradation increases estrogenicity of textile wastewater in biological treatment systems. Water Research, 184, 116137.
5. Li, Y., Wang, Y., 2019. Double decoupling effectiveness of water consumption and wastewater discharge in china's textile industry based on water footprint theory. PeerJ, 7, e6937.
6. Antczak, A., Greta, M., Kopeć, A., Otto, J., 2019. Characteristics of the textile industry of two Asian powers: China and India. Prospects for Their Further Development on Global Markets. Fibers & Textiles in Eastern Europe.
7. Mikac, L., Marić, I., Štefanić, G., Jurkin, T., Ivanda, M., Gotić, M., 2019. Radiolytic synthesis of manganese oxides and their ability to decolorize methylene blue in aqueous solutions. Applied Surface Science, 476, 1086-1095.
8. Asgari, G., Shabanloo, A., Salari, M., Eslami, F., 2020. Sonophotocatalytic treatment of AB113 dye and real textile wastewater using ZnO/Persulfate: modeling by response surface methodology and artificial neural network. Environmental Research, 184, 109367.
9. Jorfi, S., Pourfadakari, S., Kakavandi, B., 2018. A new approach in sono-photocatalytic degradation of recalcitrant textile wastewater using MgO@Zeolite nanostructure under UVA irradiation. Chemical Engineering Journal, 343, 95-107.
10. Giwa, A., Yusuf, A., Balogun, H.A., Sambudi, N.S., Bilad, M.R., Adeyemi, I., Curcio, S., 2021. Recent advances in advanced oxidation processes for removal of contaminants from water: a comprehensive review. Process Safety and Environmental Protection.
11. Doumic, L.I., Soares, P.A., Ayude, M.A., Cassanello, M., Boaventura, R.A., Vilar, V.J., 2015. Enhancement of a solar photo-fenton reaction by using ferrioxalate complexes for the treatment of a synthetic cotton-textile dyeing wastewater. Chemical Engineering Journal, 277, 86-96.

12. Garrido-Cardenas, J.A., Esteban-García, B., Agüera, A., Sánchez-Pérez, J.A., Manzano-Agugliaro, F., 2020. Wastewater treatment by advanced oxidation process and their worldwide research trends. International Journal of Environmental Research and Public Health, 17(1), 170.
13. Ma, S., Lee, S., Kim, K., Im, J., Jeon, H., 2021. Purification of organic pollutants in cationic thiazine and azo dye solutions using plasma-based advanced oxidation process via submerged multi-hole dielectric barrier discharge. Separation and Purification Technology, 255, 117715.
14. Sampaio, E.F., Rodrigues, C.S., Lima, V.N., Madeira, L.M., 2021. Industrial wastewater treatment using a bubble photo-fenton reactor with continuous gas supply. Environmental Science and Pollution Research, 28(6), 6437-6449.
15. Ribeiro, J.P., Marques, C.C., Portugal, I., Nunes, M.I., 2020b. AOX removal from pulp and paper wastewater by fenton and photo-fenton processes: a real case study. Energy Reports, 6, 770-775.
16. Liu, R., Chiu, H.M., Shiau, C.S., Yeh, R.Y.L., Hung, Y.T., 2007. Degradation and sludge production of textile dyes by fenton and photo-fenton processes. Dyes and Pigments, 73(1), 1-6.
17. Fenton, H.J.H., 1894. LXXIII-oxidation of tartaric acid in presence of iron. Journal of the Chemical Society, Transactions, 65, 899-910.
18. Walling, C., 1975. Fenton's reagent revisited. Accounts of Chemical Research, 8(4), 125-131.
19. Zhang, H., Choi, H.J., Huang, C.P., 2005. Optimization of fenton process for the treatment of landfill leachate. Journal of Hazardous Materials, 125(1-3), 166-174.
20. Rodrigues, C.S., Neto, A.R., Duda, R.M., de Oliveira, R.A., Boaventura, R.A., Madeira, L.M., 2017. Combination of chemical coagulation, photo-fenton oxidation and biodegradation for the treatment of vinasse from sugar cane ethanol distillery. Journal of Cleaner Production, 142, 3634-3644.
21. Barros, V.G., Rodrigues, C.S.D., Botello-Suarez, W.A., Dudu, R.M., Oliveira, R.A., Silva,E.S., Faria, J.L., Boaventura, R.A.R., Madeira, L.M., 2020. Treatment of biodigested coffee processing wastewater using fenton's oxidation and coagulation/flocculation. Environmental Pollution, 259, 113796.
22. Yu, X., Somoza-Tornos, A., Graells, M., Pérez-Moya, M., 2020. An experimental approach to the optimization of the dosage of hydrogen peroxide for fenton and photo-fenton processes. Science of the Total Environment, 743, 140402.
23. Ribeiro, J.P., Marques, C.C., Portugal, I., Nunes, M.I., 2020a. Fenton processes for AOX removal from a kraft pulp bleaching industrial wastewater: optimization of operating conditions and cost assessment. Journal of Environmental Chemical Engineering, 8(4), 104032.
24. Silva, L.G., Moreira, F.C., Cechinel, M.A.P., Mazur, L.P., de Souza, A.A.U., Souza, S.M.G.U., Vilar, V.J., 2020. Integration of fenton's reaction based processes and cation exchange processes in textile wastewater treatment as a strategy for water reuse. Journal of Environmental Management, 272, 111082.
25. Elmolla, E.S., Chaudhuri, M., Eltoukhy, M.M., 2010. The use of artificial neural network (ANN) for modeling of COD removal from antibiotic aqueous solution by the fenton process. Journal of Hazardous Materials, 179(1-3), 127-134.
26. Radwan, M., Alalm, M.G., Eletriby, H., 2018. Optimization and modeling of electro-fenton process for treatment of phenolic wastewater using nickel and sacrificial stainless steel anodes. Journal of Water Process Engineering, 22, 155-162.
27. Talwar, S., Verma, A.K., Sangal, V.K., 2019. Modeling and optimization of fixed mode dual effect (photocatalysis and photo-fenton) assisted metronidazole degradation using ANN coupled with genetic algorithm. Journal of Environmental Management, 250, 109428.
28. Gholizadeh, A.M., Zarei, M., Ebratkhahan, M., Hasanzadeh, A., 2021. Phenazopyridine degradation by electro-fenton process with magnetite nanoparticles-activated carbon cathode, artificial neural networks modeling. Journal of Environmental Chemical Engineering, 9(1), 104999.
29. Baştürk, E., Alver, A., 2019. Modeling azo dye removal by sono-fenton processes using response surface methodology and artificial neural network approaches. Journal of Environmental Management, 248, 109300.
30. Mohammadi, F., Bina, B., Karimi, H., Rahimi, S., Yavari, Z., 2020. Modeling and sensitivity analysis of the alkylphenols removal via moving bed biofilm reactor using artificial neural networks: comparison of levenberg marquardt and particle swarm optimization training algorithms. Biochemical Engineering Journal, 161, 107685.
31. Ahmad, Z.U., Yao, L., Islam, F., Zappi, M.E., Gang, D.D., 2020. The use of artificial neural network (ANN) for modeling the adsorption of sunset yellow onto neodymium-modified ordered mesoporous carbon. Chemosphere, 256, 127081.

32. Bousalah, D., Zazoua, H., Boudjemaa, A., Benmounah, A., Bachari, K., 2020. Degradation of indigotine food dye by fenton and photo-fenton processes. International Journal of Environmental Analytical Chemistry, 1-14.
33. MathWorks, 2020. Matlab deep learning toolbox release 2020a. Natick, Massachusetts, United States. License Number, 968398.
34. APHA, 2017. Standard methods for the examination of water and wastewater (23rd ed.). American Public Health Association. Washington DC. ISSN, 55-1979.
35. Levenberg, K., 1944. A Method for the solution of certain nonlinear problems. Q. Appl. Math., 2, 164-168.
36. Yu, H., Wilamowski, B.M., 2011. Industrial electronics handbook. Levenberg-Marquadt Training.
37. Khaki, M., Yusoff, I., Islami, N., 2015. Application of the artificial neural network and neuro-fuzzy system for assessment of groundwater quality. Clean–Soil, Air, Water, 43(4), 551-560.
38. Alsumaiei, A.A., 2020. A nonlinear autoregressive modeling approach for forecasting groundwater level fluctuation in urban aquifers. Water, 12(3), 820.
39. Bishop, C.M., 1995. Neural networks for pattern recognition. Oxford University Press. ISBN:978 0-19-853864-6.
40. Di Nunno, F., Granata, F., 2020. Groundwater level prediction in apulia region using NARX neural network. Environmental Research, 190, 110062.
41. Møller, M.F., 1993. A scaled conjugate gradient algorithm for fast supervised learning [J]. Neural Networks, 6(4), 525-534.
42. Sharma, B., Venugopalan, K., 2014. Comparison of neural network training functions for hematoma classification in brain CT images. IOSR J. Comput. Eng, 16(1), 31-35.
43. Chitsazan, M., Rahmani, G., Neyamadpour, A., 2015. Forecasting groundwater level by artificial neural networks as an alternative approach to groundwater modeling. Journal of the Geological Society of India, 85(1), 98-106.
44. Du, Y.C., Stephanus, A., 2018. Levenberg-marquardt neural network algorithm for degree of arteriovenous fistula stenosis classification using a dual optical photoplethysmography sensor. Sensors, 18(7), 2322.
45. Jawad, J., Hawari, A.H., Zaidi, S., 2020. Modeling of forward osmosis process using artificial neural networks (ANN) to predict the permeate flux. Desalination, 484, 114427.
46. Zhang, T., Barthorpe, R.J., Worden, K., 2020. On treed gaussian processes and piecewise-linear NARX modelling. Mechanical Systems and Signal Processing, 144, 106877.
47. Bararpour, S.T., Feylizadeh, M.R., Delparish, A., Qanbarzadeh, M., Raeiszadeh, M., Feilizadeh, M., 2018. Investigation of 2-nitrophenol solar degradation in the simultaneous presence of $K_2S_2O_8$ and H_2O_2: using experimental design and artificial neural network. Journal of Cleaner Production, 176, 1154-1162.
48. Kalantary, R.R., Moradi, M., Pirsaheb, M., Esrafili, A., Jafari, A.J., Gholami, M., Dragoi, E.N., 2019. Enhanced photocatalytic inactivation of E. coli by natural pyrite in presence of citrate and EDTA as effective chelating agents: experimental evaluation and kinetic and ANN models. Journal of Environmental Chemical Engineering, 7(1), 102906.
49. Mousavi, S.A., Vasseghian, Y., Bahadori, A., 2020. Evaluate the performance of fenton process for the removal of methylene blue from aqueous solution: experimental, neural network modeling and optimization. Environmental Progress & Sustainable Energy, 39(2).
50. Roudi, A.M., Kamyab, H., Chelliapan, S., Ashokkumar, V., Kumar, A., Yadav, K.K., Gupta, N., 2020. Application of response surface method for total organic carbon reduction in leachate treatment using fenton process. Environmental Technology & Innovation, 19, 101009.
51. Göde, J.N., Hoefling Souza, D., Trevisan, V., Skoronski, E., 2019. Application of the fenton and fenton-like processes in the landfill leachate tertiary treatment. Journal of Environmental Chemical Engineering, 7, 103352.
52. Bello, M.M., Raman, A.A.A., Asghar, A., 2020. Activated carbon as carrier in fluidized bed reactor for fenton oxidation of recalcitrant dye: oxidation-adsorption synergy and surface interaction. Journal of Water Process Engineering, 33, 101001.
53. Xing, L., Kong, M., Xie, X., Sun, J., Wei, D., Li, A., 2020. Feasibility and safety of papermaking wastewater in using as ecological water supplement after advanced treatment by fluidized-bed fenton coupled with large-scale constructed wetland. Science of the Total Environment, 699, 134369.
54. Masalvad, S.K.S., Sakare, P.K., 2020. Application of photo-fenton process for treatment of textile congo-red dye solution materials today, Proceedings.

55. Wu, C., Chen, W., Gu, Z., Li, Q., 2021. A review of the characteristics of fenton and ozonation systems in landfill leachate treatment. Science of the Total Environment, 762, 143131.
56. Zhai, J., Ma, H., Liao, J., Rahaman, M.H., Yang, Z., Chen, Z., 2018. Comparison of fenton, ultraviolet–fenton and ultrasonic–fenton processes on organics and colour removal from pre-treated natural gas produced water. International Journal of Environmental Science and Technology, 15(11), 2411-2422.
57. Pliego, G., Zazo J.A., Garcia-Muñoz, P., 2015. Trends in the intensification of the fenton process for wastewater treatment: an overview. Crit Rev Environ Sci Technol, 45, 2611-2692.
58. Tamimi, M., Qourzal, S., Barka, N., Assabbane, A., Ait-Ichou, Y., 2008. Methomyl degradation in aqueous solutions by fenton's reagent and the photo-fenton system. Separation and Purification Technology, 61(1), 103-108.
59. Abedinzadeh, N., Shariat, M., Monavari, S.M., Pendashteh, A., 2018. Evaluation of color and COD removal by fenton from biologically (SBR) pre-treated pulp and paper wastewater. Process Safety and Environmental Protection, 116, 82-91.
60. Sevimli, M.F., Deliktacs, E., Sahinkaya, S., Güçlü, D., 2014. A comparative study for treatment of white liquor by different applications of fenton process. Arab. J. Chem. 7, 1116-1123.
61. ZDHC Programme, 2016. Zero discharge of hazardous chemicals programme. Textile industry wastewater quality guideline. Literature Review. Revision 1, 1-84.
62. Brink, A., Sheridan, C.M., Harding, K.G., 2011. The fenton oxidation of biologically treated paper and pulp mill effluents: performance and kinetic study. Process Saf. Environ Prot., 107, 206-215.
63. Askarniya, Z., Sadeghi, M.T., Baradaran, S., 2020. Decolorization of congo red via hydrodynamic cavitation in combination with fenton's reagent. Chemical Engineering and Processing-Process Intensification, 150, 107874.
64. Gadekar, M.R., Ahammed, M.M., 2019. Modeling dye removal by adsorption onto water treatment residuals using combined response surface methodology-artificial neural network approach. Journal of Environmental Management, 231, 241-248.
65. Besliu-Ionescu, D., Talpeanu, D.C., Mierla, M., Muntean, G.M., 2019. On the prediction of geoeffectiveness of CMEs during the ascending phase of SC24 using a logistic regression method. Journal of Atmospheric and Solar-Terrestrial Physics, 193, 105036.
66. Ghaedi, A.M., Karamipour, S., Vafaei, A., Baneshi, M.M., Kiarostami, V., 2019. Optimization and modeling of simultaneous ultrasound-assisted adsorption of ternary dyes using copper oxide nanoparticles immobilized on activated carbon using response surface methodology and artificial neural network. Ultrasonics Sonochemistry, 51, 264-280.
67. Koçak, Y., Şiray, G.Ü., 2021. New activation functions for single layer feedforward neural network. Expert Systems with Applications, 164, 113977.
68. Erdem, F., 2019. S. cerevisiae ile Remazol Sarı (RR) giderimine yapay sinir ağı (YSA) Yaklaşımı. Uludağ University J. Fac. Eng. 24(2), 289-298.
69. Huo, S., Necas, D., Zhu, F., Chen, D., An, J., Zhou, N., Ruan, R., 2021. Anaerobic digestion wastewater decolorization by H_2O_2-enhanced electro-fenton coagulation following nutrients recovery via acid tolerant and protein-rich chlorella production. Chemical Engineering Journal, 406, 127160.
70. Yu, R.F., Chen, H.W., Cheng, W.P., Hsieh, P.H., 2009. Dosage control of the fenton process for color removal of textile wastewater applying ORP monitoring and artificial neural networks. Journal of Environmental Engineering, 135(5), 325-332.
71. ASCE., 2000. Task committee on application of artificial neural networks in hydrology. J. Hydrol. Eng. 5(2). 115-123.
72. Yetkin, M., Kim, Y., 2019. Time series prediction of mooring line top tension by the NARX and volterra model. Applied Ocean Research, 88, 170-186.
73. Roghanchi, P., Kocsis, K.C., 2019. Quantifying the thermal damping effect in underground vertical shafts using the nonlinear autoregressive with external input (NARX) algorithm. International Journal of Mining Science and Technology, 29(2), 255-262.